Available online at www.sciencedirect.com

ScienceDirect

Ceramics International 40 (2014) 1111–1116

CERAMICS INTERNATIONAL

www.elsevier.com/locate/ceramint

Improved electrical properties of Nd-doped $K_{0.5}Bi_{4.5}Ti_4O_{15}$ thin films prepared by chemical solution deposition

J.W. Kim[a], D. Do[b], C.M. Raghavan[a], S.S. Kim[a,*]

[a]Department of Physics, Changwon National University, Changwon, Gyeongnam 641-773, Republic of Korea
[b]Department of Advanced Materials Engineering, Keimyung University, Daegu 704-701, Republic of Korea

Received 10 May 2013; received in revised form 28 June 2013; accepted 28 June 2013
Available online 4 July 2013

Abstract

$K_{0.5}Bi_{4.5}Ti_4O_{15}$ (KBTi) and $K_{0.5}Bi_4Nd_{0.5}Ti_4O_{15}$ (KBNdT) thin films were prepared using a chemical solution deposition. For all samples, layered perovskite structures with a single phase and a good crystalline structure were observed in the X-ray diffraction patterns and the Raman scattering spectra. The microstructures were composed of fine grains without cracks in the scanning electron microscope results. The KBNdT thin film exhibited a better hysteresis loop than the KBTi thin film. For the KBNdT thin film, the remnant polarization ($2P_r$) was 45 μC/cm^2 and the leakage current density was approximately half an order of magnitude lower than that of the KBTi thin film. In addition, no polarization fatigue was observed in the KBNdT thin film up to 4.44×10^9 switching cycles. Therefore, Nd-doping is an effective method to improve the ferroelectric properties of the KBTi thin film.

Keywords: A. Films; B. X-ray methods; C. Electrical properties; C. Ferroelectric properties

1. Introduction

Bismuth layer-structured ferroelectrics (BLSFs) are nontoxic lead-free ferroelectric materials. BLSF thin films have been extensively investigated for integrated device applications, such as nonvolatile ferroelectric random access memories (NvFeRAMs) [1,2]. For the NvFeRAMs device application, ferroelectric materials should satisfy the following requirements: large remnant polarization, small coercive field, fatigue-free with metal electrode and low processing temperature [3]. The crystal structure of BLSFs is generally formulated as $(Bi_2O_2)^{2+}(A_{m-1}B_mO_{3m+1})^{2-}$, where A represents Bi^{3+}, Sr^{2+}, K^+, Na^+, etc., B represents Ti^{4+}, Ta^{5+}, Nb^{5+}, etc., and m is the number of BO_6 octahedra in the pseudo-peroviskite blocks ($m=1$, 2, 3, 4, 5 and 6). The perovskite blocks, which are $(A_{m-1}B_mO_{3m+1})^{2-}$ layers, are sandwiched between bismuth oxide layers, $(Bi_2O_2)^{2+}$, along the c-axis in a unit cell [3,4]. Typical examples of the first 4 numbers of this series are Bi_2MoO_6 (m=1), $SrBi_2Ta_2O_9$ (SBT, m=2), $Bi_4Ti_3O_{12}$ (BIT, m=3) and $SrBi_4Ti_4O_{15}$ (m=4).

Among them, SBT shows excellent endurance against polarization switching after over 10^{10} cycles with the Pt electrode. However, SBT has a small remnant polarization ($2P_r$) (typically 4–16 μC/cm^2) and higher processing temperature (750–800 °C) [5,6]. Another BLSFs family, BIT has a lower processing temperature than other BLSFs. However, the BIT thin film capacitor with Pt electrode suffers from a high leakage current density and poor fatigue properties [7]. Recently, it was reported that A-site doped, B-site doped or A-, B-sites co-doped BIT thin films showed good ferroelectric properties [8–11]. In the case of A-site doped BIT, Chon et al. reported that Nd-doped BIT thin film has a large $2P_r$ (~100 μC/cm^2) and fatigue-free characteristic with Pt electrodes [10].

In general, larger polarization is expected for BLSFs with more BO_6 octahedra (m) in a unit cell [12]. Recently $K_{0.5}Bi_{4.5}Ti_4O_{15}$, which is a BLSF with $m=4$, has been studied and a large remnant polarization (P_r) of 31 μC/cm^2 and a small coercive field (106 kV/cm) were reported in $K_{0.5}Bi_{4.5}Ti_4O_{15}$ single crystals [13]. However, almost no property of $K_{0.5}Bi_{4.5}Ti_4O_{15}$ thin film is reported. In this study, $K_{0.5}Bi_{4.5}Ti_4O_{15}$ and $K_{0.5}Bi_4Nd_{0.5}Ti_4O_{15}$ thin films were prepared on Pt(111)/Ti/SiO_2/Si(100) substrates using a chemical solution deposition method. The effects of Nd-doping on the

*Corresponding author. Tel.: +82 55 213 3421; fax: +82 55 267 0264.
E-mail address: sskim@changwon.ac.kr (S.S. Kim).

0272-8842/$ - see front matter © 2013 Elsevier Ltd and Techna Group S.r.l. All rights reserved.
http://dx.doi.org/10.1016/j.ceramint.2013.06.111

structure and the electrical properties of the $K_{0.5}Bi_{4.5}Ti_4O_{15}$ thin films were systematically investigated and the results are discussed in detail.

2. Experimental procedure

$K_{0.5}Bi_{4.5}Ti_4O_{15}$ (KBTi) and $K_{0.5}Bi_4Nd_{0.5}Ti_4O_{15}$ (KBNdT) thin films were deposited on Pt(111)/Ti/SiO_2/Si(100) substrates using a chemical solution deposition method. For the KBNdT, potassium nitrate [KNO_3], bismuth nitrate pentahydrate [$Bi(NO_3)_3 \cdot 5H_2O$], titanium isopropoxide [$Ti[OCH(CH_3)_2]_4$] and neodymium nitrate hexahydrate [$Nd(NO_3)_3 \cdot 6H_2O$] were used as the starting materials for the precursor solution. 2-methoxyethanol (2-MOE) and acetic acid were used as a solvent and a catalyst, respectively. Potassium nitrate was completely dissolved in 2-MOE at 40 °C and stirred for 30 min. Acetic acid was added to this solution and stirred for 30 min. Bismuth nitrate pentahydrate (10 mol % excess) and neodymium nitrate hexahydrate were dissolved into the above potassium solution and stirred for 2 h. Separately, 2-MOE and acetylacetone were mixed at room temperature in a glove box for 30 min to make a homogeneous solution. Acetylacetone was used as a chelating agent. Titanium isopropoxide was dissolved in 2-MOE-acetylacetone and then stirred for 1.5 h. The titanium solution was added to the potassium–bismuth–neodymium solution with continuous stirring at room temperature, and the final mixture was stirred for an additional 3 h. The concentration of KBNdT in the final solution was adjusted to approximately 0.1 M. For the reference, a KBTi solution was also prepared using the same method.

A spin-coating method was used to deposit the KBTi and the KBNdT thin films on-to the Pt(111)/Ti/SiO_2/Si(100) substrates at an angular speed of 3500 rpm for 25 s. After spin coating, the wet film was prebaked sequentially at room temperature, 200 and 360 °C for 5 min each on a hotplate. The coating and the prebaking were repeated 15 times to obtain the desired thickness. After multiple layers were coated and prebaked, the entire thin film was heated at 500 °C for 3 min using a rapid thermal annealing (RTA) process with continuous oxygen flow. At the final stage, the thin film was annealed at 700 °C for 3 min by RTA in an oxygen atmosphere for crystallization.

The structures of the thin films were investigated using an X-ray diffractometer (Philips, X'Pert MPD 3040) and a Raman spectroscope (Jasco, NRS-3100). The surface morphologies and the film thicknesses were examined using a scanning electron microscope (Tescan, MIRA II LMH). Platinum electrodes with area of 1.54×10^{-4} cm^2 were deposited on the top surfaces of the thin films by ion sputtering through a metal shadow mask to form the capacitor structures. A precision materials analyzer (Radiant Technologies Inc., Precision LC), an LF impedance analyzer (HP, 4192 A) and an electrometer (Keithley, 6517 A) were used for the electrical measurements.

3. Results and discussion

Fig. 1 shows the X-ray diffraction (XRD) patterns of the KBTi and the KBNdT thin films prepared on Pt(111)/Ti/SiO_2/Si(100) substrates using a chemical solution deposition method followed by RTA at 700 °C for 3 min in an oxygen atmosphere. The peak positions of the KBTi and the KBNdT thin films generally correspond to the bismuth layer-structured ferroelectrics without prominent peaks, which are related to the secondary phases. The intensities of the XRD peaks show no neodymium doping effect.

The specific site substitution of Nd^{3+} ion into the KBTi thin film was investigated using a Raman scattering spectrum. Fig. 2 shows the Raman spectra of the KBTi and KBNdT thin films measured at room temperature. A solid state laser with a 532 nm excitation line was used to measure the Raman spectra. By fitting the measured spectra and decomposing the fitted curves into individual Lorentz components, we obtained the peak positions. For BLSFs, the Raman active modes are reported to originate from the internal vibration of the TiO_6 octahedra and the lattice transition, which is caused by the cationic motion in the pseudo-perovskite blocks. The Raman modes observed between 90 and 200 cm^{-1} are related to the vibrations of the A-site ions (K, Bi) in the pseudo-perovskite blocks. The mode at 269 cm^{-1} and the modes from 550 to 850 cm^{-1} are the torsional bending and the stretching modes of the TiO_6 octahedra, respectively [14–16]. The assigned Raman active modes for the KBTi and the KBNdT thin films are provided in Table 1. From Table 1, slight changes in the Raman modes were observed for the KBNdT compared to the KBTi. The Nd^{3+} ion doping into the Bi-site might lead to the dispersion of the Bi–O (343 kJ/cm) bond in the perovskite layer because of the strong Nd–O (703 kJ/mol) bond energy. The significant shifts in the Raman peaks at approximately 500–800 cm^{-1} imply that Nd^{3+} doping might lead to the crystallographic distortion of the TiO_6 octahedra in the KBNdT. Thus, the internal stress induced in the lattices of the pseudo-perovskite blocks by Nd^{3+} doping leads to local disorders in the layered structure [16]. A similar result in the

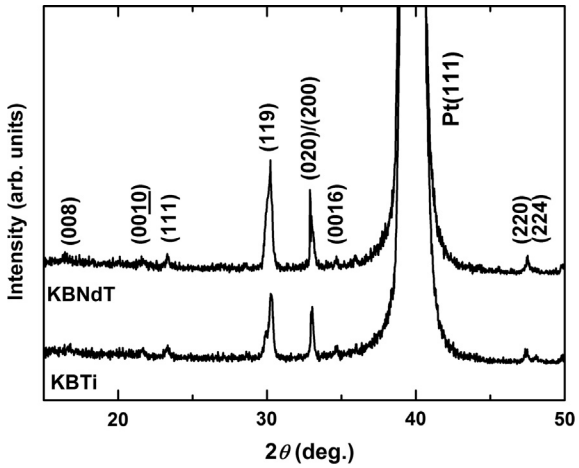

Fig. 1. X-ray diffraction patterns of the KBTi and the KBNdT thin films fabricated on Pt(111)/Ti/SiO_2/Si(100) substrates.

Table 1
The decomposed Raman active modes of the KBTi and the KBNdT thin films.

	Frequencies (cm^{-1})									
	ν_1	ν_2	ν_3	ν_4	ν_5	ν_6	ν_7	ν_8	ν_9	ν_{10}
KBTi	123.4	147.2	183.2	223.0	269.1	332.1	548.9	576.8	621.4	847.9
KBNdT	124.5	148.9	183.2	223.2	269.3	332.1	559.7	585.9	635.0	849.2

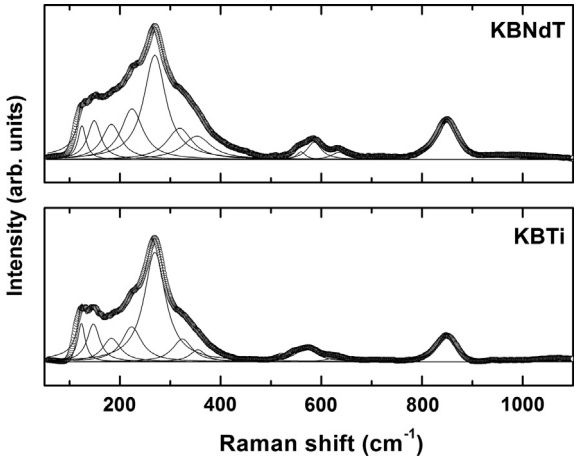

Fig. 2. Raman scattering spectra and decomposed active modes for the KBTi and the KBTFe thin films measured at room temperature.

Raman scattering spectrum was observed in Gd-doped $Na_{0.5}Bi_{4.5}Ti_4O_{15}$ [15].

The changes in microstructure with the Nd-doping effect are shown in Fig. 3. Both the KBTi and the KBNdT thin films have dense surfaces without any evidence of cracks. The average grain sizes of the thin films are different. The KBNdT thin film has a larger grain size than the KBTi thin film (KBTi: ~130 nm, and KBNdT: ~155 nm). The ferroelectric properties of the BLSF thin films depend on the grain size. The BLSF thin film with the large grain size exhibits better ferroelectric properties [17]. Thus we expect that the KBNdT thin film has better ferroelectric properties than the KBTi thin film. The thickness of each thin film was approximately 300 nm.

Fig. 4(a) shows the hysteresis loops of the KBTi and the KBNdT thin films measured at maximum applied electric fields. The KBNdT thin film shows better hysteresis loops than the KBTi thin film. The broken-down electric fields of the KBTi and the KBNdT thin films were 300 kV/cm and 500 kV/cm, respectively. It has been reported that the values of the remnant polarization ($2P_r$) and coercive field ($2E_c$) of ferroelectric materials are affected by many factors [18–20]. In this case, Nd-doping suppresses the volatility of Bi and increases the stability of the TiO_6 octahedral in the KBTi thin film [21]. Fig. 4(b) shows $2P_r$ values of the KBTi and the KBNdT thin films as functions of the applied electric fields. The $2P_r$ values increased with increasing applied electric field. The $2P_r$ values of the KBTi and the KBNdT thin films were 13.5 μC/cm^2 and 19.2 μC/cm^2, respectively, at an applied electric field of 230 kV/cm. At an applied electric field of 430 kV/cm, the $2P_r$ values of the KBNdT thin film was 45.2 μC/cm^2. Fig. 4(c) shows the $2E_c$ values of the KBTi and the KBNdT thin films as functions of the applied electric fields. The $2E_c$ values of the KBTi and the KBNdT thin films were 155 kV/cm and 125 kV/cm, respectively, at an applied electric field of 230 kV/cm.

The frequency dependences of the dielectric constants (ε) and the dielectric losses ($\tan\delta$) of the KBTi and the KBNdT thin films measured at room temperature are shown in Fig. 5. The measurement was performed in the frequency range of

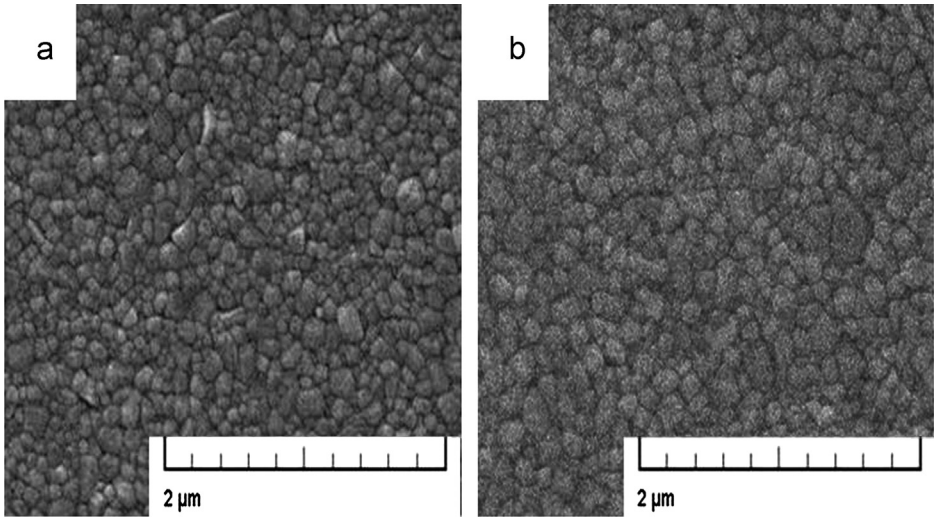

Fig. 3. SEM surface morphologies of the (a) KBTi and the (b) KBNdT thin films.

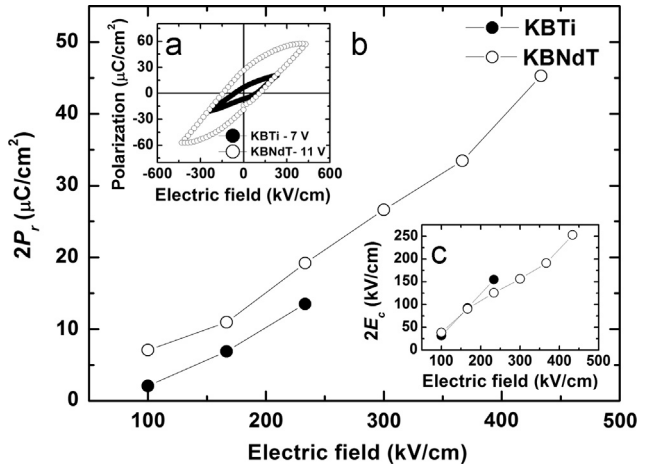

Fig. 4. (a) Ferroelectric hysteresis loops of the KBTi and the KBNdT thin films, (b) and (c) Electric field dependences of the remnant polarization ($2P_r$) and the coercive field ($2E_c$) of the KBTi and the KBNdT thin films, respectively.

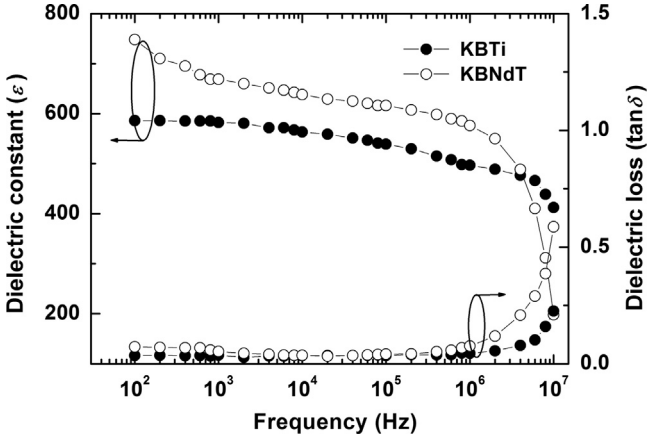

Fig. 5. Dielectric properties of the KBTi and the KBNdT thin films.

100 Hz–10 MHz. At 1 kHz, the dielectric constants of the KBTi and the KBNdT thin films were 582 and 668, respectively. At 1 kHz, the dielectric losses of the KBTi and the KBNdT thin films were 0.03 and 0.05, respectively.

Fig. 6(a) shows the plots of leakage current density versus the applied electric field (*J*–*E*) of the KBTi and the KBNdT thin films measured at room temperature. The KBTi and the KBNdT thin films have similar *J*–*E* behaviors. The measured leakage current densities of the KBTi and the KBNdT thin films were 5.74×10^{-7} and 2.64×10^{-8} A/cm^2, respectively, at an external electric field of 100 kV/cm. Various mechanisms to detect a current in insulating thin films, such as space charge limited conduction (SCLC), Schottky emission and Poole–Frenkel emission, have been previously proposed [22]. The leakage current mechanisms for the KBTi and the KBNdT thin films were analyzed using logarithmic plots of current density versus applied electric field (log(*J*)–log(*E*)) as shown in Fig. 6 (b). In the low electric field region, the KBTi and the KBNdT thin films follow the Ohmic conduction mechanism. However, for higher applied electric fields, the characteristics exhibit nonlinear behaviors. An instant look at the natures of the curves indicate that the conduction behaviors for both thin films follow Lampert's theory [23] of the SCLC current. Three regions with different slopes, which are governed by different conduction mechanisms, are clearly distinguishable. These three regions formed triangles that are called 'Lampert triangles' [24]. The different regions can be represented by Ohm's law, trap-filled limited conduction and Child's law. For applied electric fields up to 99 kV/cm for the KBTi thin film and 119 kV/cm for the KBNdT thin film, the curves obey Ohm's law. The onsets of trap-filled limited conduction occur when the applied electric fields are 99 kV/cm and 119 kV/cm, and the mechanism is dominant up to 126 kV/cm and 143 kV/cm for the KBTi thin film and the KBNdT thin film, respectively. When the applied electric fields are higher than 126 kV/cm and 143 kV/cm, the current conduction mechanism

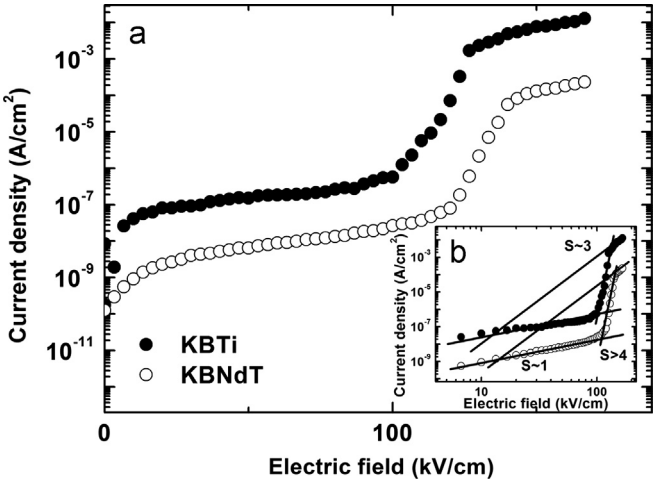

Fig. 6. (a) Leakage current density versus electric field of the KBTi and the KBNdT thin films, and (b) Log(J)–log(E) characteristics of each film showing the conduction mechanisms.

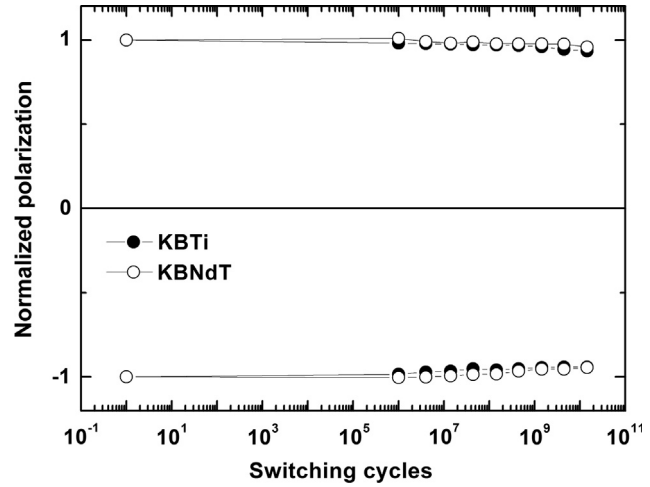

Fig. 7. Fatigue characteristics of the KBTi and the KBNdT thin films as a function of the switching cycles.

is dominated by Child's law. Therefore, the total leakage current can be represented by [22,25]

$$J = J_{Ohm} + J_{TFL} + J_{Child},$$

where

$$J_{Ohm} = e\mu n_0(V/d),\ J_{TFL} = K\left(\frac{V^{l+1}}{d^{2l+1}}\right) \text{ and } J_{Child} = \frac{9}{8}\varepsilon_0\varepsilon_r\mu\left(\frac{V^2}{d^3}\right),$$

where e is the electronic charge, μ is the carrier mobility, n_0 is the concentration of free charge carriers, d is the film thickness, ε_0 is the free space permittivity, ε_r is the high frequency dielectric constant, and V is the voltage across the thin film. In addition, $l = (T_t/T)$, where T_t is the temperature parameter that characterizes the trap distribution, and T is the absolute temperature. This result confirms the validity of the SCLC to the leakage current behaviors of our thin films.

As shown in Fig. 7, the switchable polarizations ($P^* - \hat{P}$) of the KBTi and the KBNdT thin films as functions of the switching cycles were measured at 1 MHz with maximum voltages of ± 10 V. The $+(P^* - \hat{P})$ or $-(P^* - \hat{P})$ denotes the switchable polarization, which is an important variable for nonvolatile memory application. The switchable polarization of the KBNdT thin film was approximately constant up to 4.44×10^9 cycles. The polarizations of the KBTi and the KBNdT thin films decreased to approximately 5% of the initial value after 1.4×10^{10} switching cycles.

The ferroelectric properties of BLSF thin film are influenced by the bismuth vacancies that are accompanied by the oxygen vacancies. The bond strength of Nd–O (703 kJ/mol) is larger than that of Bi–O (337 kJ/mol). Hence, the substitution of Nd into Bi-site of the KBTi thin film controls the bismuth evaporation and stabilizes the perovskite layers [26]. And the electronegativity of Nd (1.14) is lower than those of Bi (2.02) and O (3.44). Therefore, the electronegativity difference between Nd and O is higher than that of Bi and O, which in turn strengthens the Bi(Nd)–O bond and stabilizes the perovskite structure [27]. In this study, Nd-doping suppresses the volatility of Bi and increases the stability of the TiO_6 octahedral in the KBTi thin film. Thus, we conclude that the properties of the KBNdT thin film improve because the defects, such as bismuth and oxygen vacancies, are reduced by Nd^{3+} doping.

4. Conclusions

Ferroelectric $K_{0.5}Bi_{4.5}Ti_4O_{15}$ (KBTi) and $K_{0.5}Bi_4Nd_{0.5}Ti_4O_{15}$ (KBNdT) thin films were prepared on Pt(111)/Ti/SiO_2/Si substrates using a chemical solution deposition method and annealed using an RTA process at 700 °C for 3 min in an oxygen atmosphere. The $2P_r$ and $2E_c$ values of the KBNdT thin film were 45.2 μC/cm^2 and 253 kV/cm, respectively, at an electric field of 430 kV/cm. The dielectric constant and the dielectric loss of the KBNdT thin film were 668 and 0.05, respectively, at 1 kHz. The leakage current density of the KBNdT thin film was 1.16×10^{-7} A/cm^2 at an external electric field of 100 kV/cm. The switchable polarization of the thin film was reasonably unchanged up to 4.44×10^9 switching cycles. We conclude that the properties of the KBNdT thin film improve because the defects, such as bismuth and oxygen vacancies, are reduced by Nd^{3+} doping.

Acknowledgments

This work was supported by the Priority Research Centers Program through the National Research Foundation of Korea (NRF) funded by the Ministry of Education, Science and Technology (2010-0029634).

References

[1] Z.-G. Gai, J.-F. Wang, M.-L. Zhao, C.-M. Wang, G.-Z Zang, B.-Q. Ming, P. Qi, S. Zhang, T.R. Shrout, High temperature $(NaBi)_{0.48}\square_{0.04}Bi_2Nb_2O_9$-based piezoelectric ceramics, Applied Physics Letters 89 (2006) 012907.
[2] J.F. Scott, Applications of modern ferroelectrics, Science 315 (2006) 954–959.

[3] J. Zhu, W.P. Lu, X.Y. Mao, R. Hui, X.B. Chen, Study on properties of lanthanum doped $SrBi_4Ti_4O_{15}$ and $Sr_2Bi_4Ti_5O_{18}$ ferroelectric ceramics, Japanese Journal of Applied Physics 42 (2003) 5165–5168.
[4] T. Watanabe, H. Funakubo, Controlled crystal growth of layered-perovskite thin films as an approach to study their basic properties, Journal of Applied Physics 100 (2006) 051602.
[5] T. Li, T. Zhu, S.B. Desu, C.H. Peng, M. Nagata, Metalorganic chemical vapor deposition of ferroelectric $SrBi_2Ta_2O_9$ thin films, Applied Physics Letters 68 (1996) 616–618.
[6] R. Dat, J.K. Lee, O. Auciello, A.I. Kingon, Pulsed laser ablation synthesis and characterization of layered Pt/$SrBi_2Ta_2O_9$/Pt ferroelectric capacitors with practically no polarization fatigue, Applied Physics Letters 67 (1995) 572–574.
[7] T. Watanabe, A. Saiki, K. Saito, H. Fanakubo, Film thickness dependence of ferroelectric properties of *c*-axis-oriented epitaxial $Bi_4Ti_3O_{12}$ thin films prepared by metalorganic chemical vapor deposition, Journal of Applied Physics 89 (2001) 3934–3938.
[8] B.H. Park, B.S. Kang, S.D. Bu, T.W. Noh, J. Lee, W. Jo, Lanthanum-substituted bismuth titanate for use in non-volatile memories, Nature 401 (1996) 682–684.
[9] E.K. Choi, S.S. Kim, J.K. Kim, J.C. Bae, W.J. Kim, Y.I. Lee, T.K. Song, Effects of donor ion doping on the orientation and ferroelectric properties of bismuth titanate thin films, Japanese Journal of Applied Physics 43 (2004) 237–241.
[10] J.S. Kim, Y.S. Kim, B.C. Choi, J.H. Jeong, S.T. Chung, S.B. Cho, Effect of Nd and Nd/Nb doping on dielectric, ferroelectric and electrical properties of $Bi_4Ti_3O_{12}$ ceramics, Journal of Korean Physics Society 54 (2009) 906–910.
[11] Y.M. Chen, R.J. Zhang, Y.X. Zheng, P.H. Mao, W.J. Lu, L.Y. Chen, Study of the optical properties of $Bi_{3.15}Nd_{0.85}Ti_3O_{12}$ ferroelectric thin films, Journal of Korean Physics Society 53 (2008) 2299–2302.
[12] U. Chon, H.M. Jang, M.G. Kim, C.H. Chang, Layered perovskites with giant spontaneous polarizations for nonvolatile memories, Physical Review Letters 89 (2002) 087601.
[13] Y. Noguchi, M. Suzuki, Y. Kitanaka, S. Teranishi, M. Miyayama, Ferroelectric polarization and piezoelectric properties of layer-structured $K_{0.5}Bi_{4.5}Ti_4O_{15}$ single crystals, Applied Physics Letters 93 (2008) 032904.
[14] S. Kojima, R. Imaizumi, S. Hamazaki, M. Takashige, Raman study of ferroelectric bismuth layer-oxides $ABi_4Ti_40_{15}$, Journal of Molecular Structure 348 (1995) 37–40.
[15] J. Liu, Z. Zou, Y. Jin, Raman scattering study of $Na_{0.5}Bi_{4.5}Ti_40_{15}$ and its solid solutions, Journal of Physics and Chemistry of Solids 57 (1996) 1653–1658.
[16] J. Zhu, X.B. Chen, J.H. He, J.C. Shen, Investigations on Raman and X-ray photoemission scattering patterns of vanadium-doped $SrBi_4Ti_4O_{15}$ ferroelectric ceramics, Physics Letters A 362 (2007) 471–475.
[17] F. Yan, P. Bao, H.L.W. Chan, C.L. Choy, Y. Wang, The grain size effect of $Pb(Zr_{0.3}Ti_{0.7})O_3$ thin films, Thin Solid Films 406 (2002) 282–285.
[18] S.S. Kim, T.K. Song, J.K. Kim, J. Kim, Ferroelectric properties of vanadium-doped $Bi_4Ti_3O_{12}$ thin films deposited by a sol–gel method, Journal of Applied Physics 92 (2002) 2213–2215.
[19] H. Irie, M. Miyayama, Dielectric and ferroelectric properties of $SrBi_4Ti_4O_{15}$ single crystals, Applied Physics Letters 79 (2001) 251–253.
[20] J.K. Yang, W.S. Kim, H.H. Park, Effect of grain size of $Pb(Zr_{0.4}Ti_{0.6})O_3$ sol–gel derived thin films on the ferroelectric properties, Applied Surface Science 169 (2007) 544–548.
[21] M. Grossmann, O. Lohse, D. Bolten, U. Boettger, T. Schneller, R. Waser, The interface screening model as origin of imprint in $PbZr_xTi_{1-x}O_3$ thin films. I. Dopant, illumination, and bias dependence, Journal of Applied Physics 92 (2002) 2680–2687.
[22] A. Roy, S. Maity, A. Dhar, D. Bhattacharya, S.K. Ray, Temperature dependent leakage current behavior of pulsed laser ablated $SrBi_2Ta_2O_9$ thin films, Journal of Applied Physics 105 (2009) 044103.
[23] M.A. Lampert, Simplified theory of space-charge-limited currents in an insulator with traps, Physical Review 103 (1956) 1648.
[24] M.A. Lampert, Current Injection in Solids, Academic, New York, 1970.
[25] K.C. Kao, W. Hwang, Electrical Transport in Solids, Pergamon, New York, 1981.
[26] J.A. Dean, Lange's Hand book of Chemistry, 15th ed., McGraw-Hill, New York, 1999.
[27] V.V. Lazenka, M. Lorenz, H. Modarresi, K. Brachwitz, P. Schwinkendorf, T. Böntgen, J. Vanacken, M. Ziese, M. Grundmann, V.V. Moshchalkov, Effect of rare-earth ion doping on the multiferroic properties of $BiFeO_3$ thin films grown epitaxially on $SrTiO_3$(100), Journal of Physics D: Applied Physics 46 (2013) 175006.